Journal of Materials Chemistry A

Scalable synthesis of CuInS2 nanocrystal inks for photovoltaic applications

Journal:	*Journal of Materials Chemistry A*
Manuscript ID:	TA-ART-10-2014-005696.R1
Article Type:	Paper
Date Submitted by the Author:	15-Dec-2014
Complete List of Authors:	Roggan, Stefan; Bayer Technology Services, Ahlswede, Erik; Zentrum für Sonnenenergie- und Wasserstoff-Forschung Baden-Württemberg, Niyamakom, Phenwisa; Bayer Technology Services, Köhler, Karen; Bayer Technology Services, Cemernjak, Marco; Zentrum für Sonnenenergie- und Wasserstoff-Forschung Baden-Württemberg, Quintilla, Aina; Karlsruhe Institute of Technology,

Journal Name

RSCPublishing

ARTICLE

Scalable synthesis of $CuInS_2$ nanocrystal inks for photovoltaic applications

Cite this: DOI: 10.1039/xoxxoooooox

P. Niyamakom,[a] A. Quintilla,[#b] K. Köhler,[a] M. Cemernjak,[b] E. Ahlswede[*b] and S. Roggan[*a]

Received ooth January 2012,
Accepted ooth January 2012

DOI: 10.1039/xoxxoooooox

www.rsc.org/

Chalkopyrite copper indium disulfide ($CuInS_2$, CIS) nanoparticles in the range of 10 nm particle size have been prepared via hot-injection and precipitation by an easily scalable synthesis. The influence of reaction time and precursor composition on the nanoparticle properties was assessed. After surface ligand exchange CIS nanoparticle inks were deposited as thin precursor layers for $CuIn(S,Se)_2$ (CISSe) solar cells. Film formation, morphology and crystallinity after exposure of the CIS precursor layer to selenium vapour at elevated temperature have been investigated. Application of CIS precursors allows for a better control of the film composition, the lattice volume expansion by the exchange of S by Se during the selenization process minimizes the risk of voids. Solar cells made from CIS nanocrystal precursors gave power conversion efficiencies of up to 6.5% under standard AM1.5 illumination.

Introduction

$Cu(In,Ga)Se_2$ (CIGSe)-based solar cells are the most efficient of all thin-film solar cells with record values for power conversion up to 21.7 % thereby outperforming the best laboratory values of the currently market leading poly-Si solar cells.[1] CIGSe layers are conventionally deposited in high vacuum using either thermal co-evaporation of the elements Cu, In, Ga and Se,[2] or sequential deposition of the metals Cu, In and Ga with subsequent selenization.[3,4] In recent years the vacuum-free deposition of suitable precursor pastes has attracted increasing attention due to the possibility of low-cost and high-throughput large scale production of CIGSe thin-film solar cells by reducing capital investment and increasing material utillization.[5,6,7] Encouraging efficiencies have already been demonstrated by research institutes (IBM 15.2 %)[8] but also solar companies (Nanosolar 17.1 %)[9] for the quaternary or pentanary material system $Cu(In,Ga)(S,Se)_2$ including both Ga and S for an optimized band gap. In this report, however, we focus on the wet chemical solar cell preparation of the simpler $CuIn(Se,S)_2$ (CISSe) system, where power conversion efficiencies up to 15 % have been obtained by vacuum deposition.[10,11] To date with wet chemical, nanoparticle based approaches efficiencies of 8.9 % and 13 % have been reached using highly toxic and explosive hydrazine solvent[12] or H_2Se gas,[13] respectively. Here, a simple and cheap selenization process using direct Se vapour is presented[14] leading to solar cells reaching efficiencies of up to 6.5 %.

There have been diverse approaches for CISSe solar cell preparation using different nanoparticles based on monometallic nanocrystals, oxides, binary or ternary sulfides or selenides.[15,16] All of them followed the concept that nanoparticles offer a better possibility to adjust the elemental composition on a submicron scale and provide a higher reactivity with regard to film formation due to their large surface to volume ratio. On the other side, drawbacks typically encountered are a high susceptibility of the particles to oxidation and the need to use surface capping ligands, solvents and, in some cases, dispersants in order to maintain a stable colloidal dispersion without particle agglomeration. After deposition of a nanoparticle ink, in the subsequent heating and selenization step all organic ingredients have to be removed in order to guarantee a high quality CISSe absorber layer. Undesired phases and high amounts of grain boundaries due to incomplete reaction and crystallisation should be avoided as grain boundaries might promote recombination losses of photo-generated charge carriers. The CISSe system presented herein allows for low residual carbon content by an optimised ligand and solvent management and an intrinsic densification of the layer structure during selenization due to crystal volume expansion when sulfur atoms are replaced by bigger selenium atoms on the respective lattice sites.

Experimental

Material Synthesis

Korgel et al. described the synthesis of tetragonal CIS nanoparticles with diameter of 6 – 12 nm.[17] In our study we modified and adapted their procedure for realizing both a synthesis at a larger scale and variation of the Cu:In ratio in the nanomaterial.

10 mmol (2.60 g) of [$Cu(acac)_2$] (acac = acteylacetonate) and 10 mmol (4.10 g) of [$In(acac)_3$] were added into a three-neck flask with 70 mL of dichlorobenzene (DCB) forming a suspension of the Cu-In -precursor materials. For the variation of Cu:In composition the amount of [$In(acac)_3$] was increased to 12 mmol and 14 mmol, respectively. A sulfur solution was prepared by adding 20 mmol (0.64 g) of elementary sulfur (S) into DCB. The two precursor mixtures were subsequently degassed by bubbling N_2 through the solutions during 30 minutes. 20 mL of N_2-degassed oleylamine (OLA) was added into the [$Cu(acac)_2$] / [$In(acac)_3$] suspension at room temperature. The dark green mixture was then heated to 110℃. The degassed sulfur solution was pre-heated to 110℃ and then added into the warm [$Cu(acac)_2$] / [$In(acac)_3$] / OLA mixture. A black solution formed, which was refluxed under nitrogen atmosphere at 180℃ during 120 minutes. The influence of reaction time on the nanomaterial obtained was studied by variation of the latter time, i.e. 1 min, 5 min, 15 min, 30 min, 60 min, 90 min. After cooling down the sample to room temperature, 500 mL of ethanol were added to induce $CuInS_2$ nanoparticle precipitation. The sample was then left standing overnight for sedimentation. Subsequently, the supernatant was decanted and the black nanoparticles isolated by centrifugation. They were washed by repeated cycles of re-dispersion (in toluene) and precipitation (with ethanol). The washed $CuInS_2$ nanoparticles were then re-dispersed in toluene. This synthesis could be further scaled up by a factor of five, i.e. employing a precursor ratio of [$Cu(acac)_2$]:[$In(acac)_3$]:S = 50:50:100 mmol. Thereby 11 g (solid content in toluene dispersion) $CuInS_2$ nanomaterial could be synthesized in one step.

Ligand exchange and surface modification of CIS nanoparticles

For ligand exchange from OLA to pyridine we followed the recipe reported by Dilek et al..[18] The as-synthesized CIS nanoparticles were redispersed in toluene and precipitated from methanol at least three times. After this washing step, the CIS nanoparticles were dispersed in n-hexane by stirring at room temperature in a glovebox for at least 24 hours. Methanol was added to the hexane solution to induce precipitation and the CIS nanoparticles were isolated by centrifugation. (I) They were then refluxed with pyridine in a nitrogen atmosphere for at least 8 hours and then precipitated by the addition of n-hexane. The surface-modified CIS nanoparticles were finally redispersed into pyridine. (II) Alternatively, the CIS nanoparticles were surface exchanged with allylamine following a similar procedure as described for pyridine: After performing the initial washing step the CIS nanoparticles were stirred in toluene overnight, precipitated with methanol and stirred in allylamine at 60-70°C. The surface-modified CIS nanoparticles were then precipitated from methanol and redispersed into chlorobenzene.

Solar cell preparation

After homogenizing in an ultrasonic bath the CIS based inks were deposited on molybdenum-coated (~ 0.5 µm) soda lime glass substrates by doctor blading to form a precursor layer of about 0.4 µm to 0.8 µm in thickness. The films were slowly dried at room temperature. Multiple coatings were applied optionally in order to deposit films with the desired thickness. In this manner various homogenous and densely packed CIS nanoparticle films without cracks were prepared on 2.6 x 7.6 cm² substrates. For selenization in elemental selenium vapour a a graphite susceptor that holds the precursor samples along with typically 0.3 g selenium pellets was put into a rapid thermal annealing system. The water-cooled reaction chamber used allowed a very fast and defined process temperature ramp. During the standard selenization process the system was flushed with nitrogen and heated up to 550°C at 5 K/s at atmospheric pressure. The temperature was held for a nominal annealing time of 3-5 min. The absorber layers were further processed with a CdS buffer layer, a ZnO window layer and a ZnO:Al layer to obtain a complete solar cell, using conventional methods as described in Ref. [19].

Characterisation

The characterization of CIS nanomaterial was carried out with transmission electron microscopy (TEM) and X-ray diffractometry (XRD) to analyze for nanoparticle size, shape and crystalline structure, respectively. Additionally, the elemental analysis by inductively coupled plasma optical emission spectrometry (ICP-OES) has been employed to determine the stoichiometric composition of the $CuInS_2$ nanoparticles.

TEM measurements. TEM measurements were performed with a FEI TECNAI 20 electron microscope operated at an acceleration voltage of 200 kV. LaB6 was used as the electron source. Digital images were taken with a side mounted CCD camera (Olympus, MegaView III). For TEM preparation a drop of a dispersion of the nanoparticles in toluene was placed on a 300 mesh holey carbon coated copper TEM-grid (plano S1471). The mean sizes of $CuInS_2$ particles were estimated from TEM micrographs by single particle measurement of at least 250 particles.

Powder XRD analysis. XRD data were acquired using a PANalytical EMPYREAN θ-2θ powder diffractometer equipped with an automatic divergence slit, solid-state detector and a spinning sample holder. Cu Kα (λ = 1.54 Å) radiation was used. The diffraction data were collected by scanning for 10 min and a rotation speed of 60 rpm.

Solar cell characterization. After coating with a doctor blade, the film morphology and film thickness were studied with a scanning electron microscope (SEM, XL30 SFEG Sirion; FEI Company). Energy dispersive x-ray spectroscopy (EDX)

measurements were carried out in the same instrument. The elemental composition of thin films was alternatively determined by X-ray fluorescence analysis (XRF) at 10^{-1} mbar on an EAGLE XXL system, equipped with an energy-dispersive Si(Li) detector and a 50 kV Rh X-ray source. These methods were also applied for the analysis of the selenized layer. Secondary neutral mass spectrometry (SNMS) analysis was conducted with a Leybold SSM 200 LHS 10 system with a focused 5 keV Ar^+ ion beam to get detailed information of the depth profile of the $CuInSe_2$ absorber after the rapid thermal process. Current–voltage (I-V) curves were measured using a Keithley 238 source-measure unit under simulated AM 1.5 global solar irradiation of a WACOM sun simulator with 100 mW/cm^2 to extract the basic solar cell characteristics from devices of 0.25 cm^2 in size.

Results and discussion

For optimized nanoparticle synthesis, ink formation and final solar cell performance various parameters have been analyzed and modified. An important parameter is the chemical composition of the final films which typically should be optimized to be slightly Cu-poor to obtain highly efficient solar cells. As the composition might change during the selenization process, the precursor layer has to be adjusted and optimized accordingly. One of the advantages of a nanoparticle approach is the possibility to tune the desired composition already at the nanoscale. To what extend the properties of the particles can be influenced and which adjustments in the ink formulation process have to be taken care of will be described below.

$CuInS_2$ mechanism of formation

$CuInS_2$ nanoparticles were prepared by mixing the metal salt precursors in OLA and DCB. A solution of elementary sulfur in DCB was added to the precursor suspension at 110°C, after which the reaction mixture was heated to reflux. In order to obtain insight into the mechanism of $CuInS_2$ formation the time during which the precursor mixture was refluxed at 180°C was varied. Samples were also taken shortly (1 min, 5 min) after injection of the sulfur solution into the [$In(acac)_3$], [$Cu(acac)_2$], OLA, DCB precursor mixture, i.e. during the period, when the reaction mixture was heated from 110°C to 180°C. TEM and XRD analyses (Figure 1) revealed that nanoparticles are formed immediately after sulfur injection (1 min). However, no $CuInS_2$ phase was formed, yet, at this early stage of the synthesis. The powder XRD diffractogram rather indicates the formation of CuS (JCPDS 006-0464) with characteristic reflexes at 29.2°, 31.8° and 48°. The reflex at 22° is not directly assignable. $CuInS_2$ formation is clearly confirmed after 15 min reaction time by the main XRD reflexes (JCPDS 089-6095). It will occur subsequently by incorporation of Indium ions and further amounts of sulfur into the CuS lattice, while oleylamine may act as the reductant for reduction of Cu(II) to Cu(I).[20] After 15 min the usual diffraction pattern for tetragonal $CuInS_2$ was observed after the typical workup procedure. Further prolongation of the reaction time up to 90 min had no remarkable effect neither on the crystal phase or nanoparticle morphology (see ESI Figure. S1). Deeper analysis of the growth mechanisms of CIS nanoparticles via intermediate formation of copper sulfide can be found in recent publications of *Kolny-Olesiak et al.*.[21]

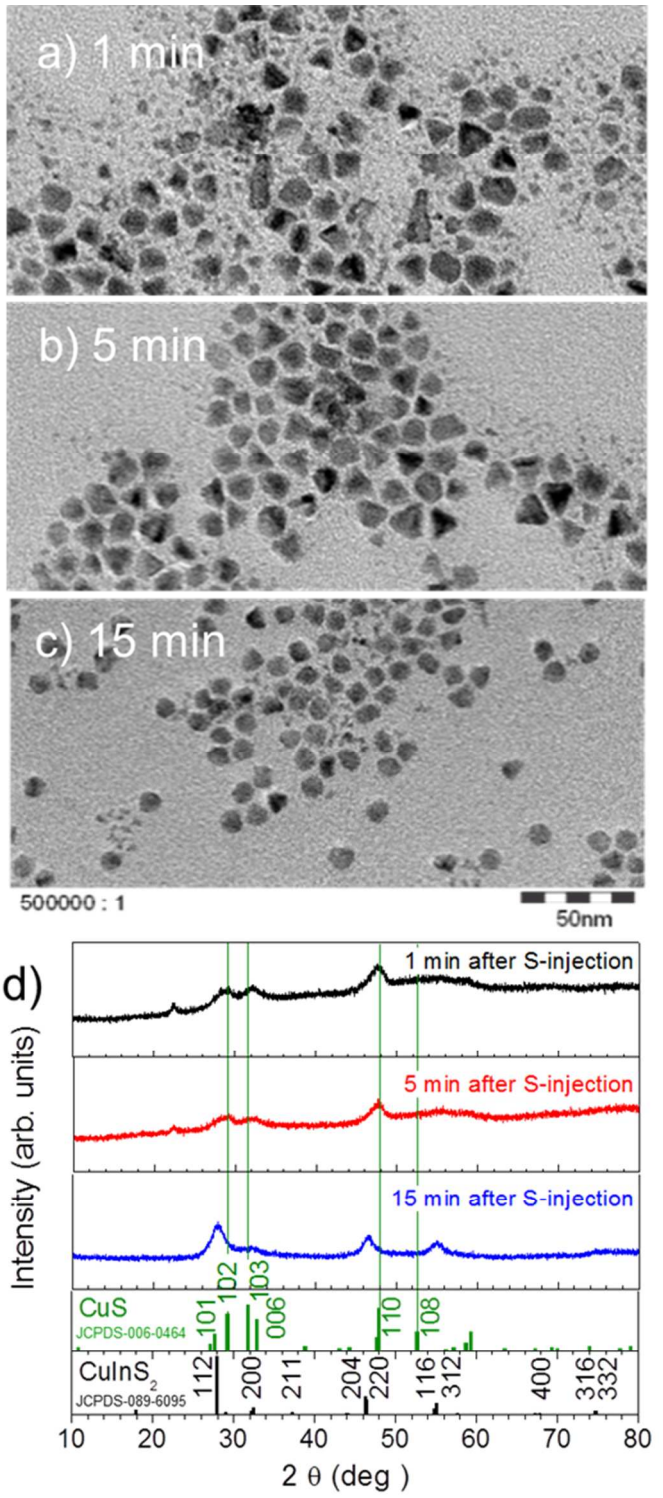

Figure 1. TEM (a,b,c) and XRD powder analyses (d) of samples taken after 1 min, 5 min, and 15 min, and XRD powder analyses of the respective samples (d). The

JCPDS reference spectra 006-0484 for CuS and 089-6095 for $CuInS_2$ are added at the bottom. Tetragonal $CuInS_2$ nanoparticles are formed after 15 min while mainly CuS nanoparticles are present in the early stage of the reaction.

Investigation of material composition

The influence on Cu:In ratio on nanoparticle synthesis was investigated for three different sample types. Table 1 summarizes the results of elemental analyses of CIS nanoparticles synthesized with varying ratios of the $[Cu(acac)_2]$ and $[In(acac)_3]$ starting materials. It is observed that when the starting material ratio of Cu:In:S corresponds to 1:1:2, Cu-rich CIS nanoparticles are mostly obtained at a – similarly as observed by Korgel *et al.* –[17] slightly substoichiometrical S content (Table 1, sample-1). The In content in as-synthesized CIS nanoparticles increases on increasing the amount of $[In(acac)_3]$ in the precursor mixture (Table 1, samples-2,3).

Table 1. Elemental analysis of $CuInS_2$ nanoparticles, synthesized with different Cu:In:S precursor ratios.

Sample	Precursor ratio $[Cu(acac)_2]$:$[In(acac)_3]$:S, [eq]	CIS composition[1]		
		Cu	In	S
1	1:1:2	1	0.96	1.88
2	1:1.2:2	1	1.06	1.72
3	1:1.4:2	1	1.16	1.88

[1]As determined by ICP-OES

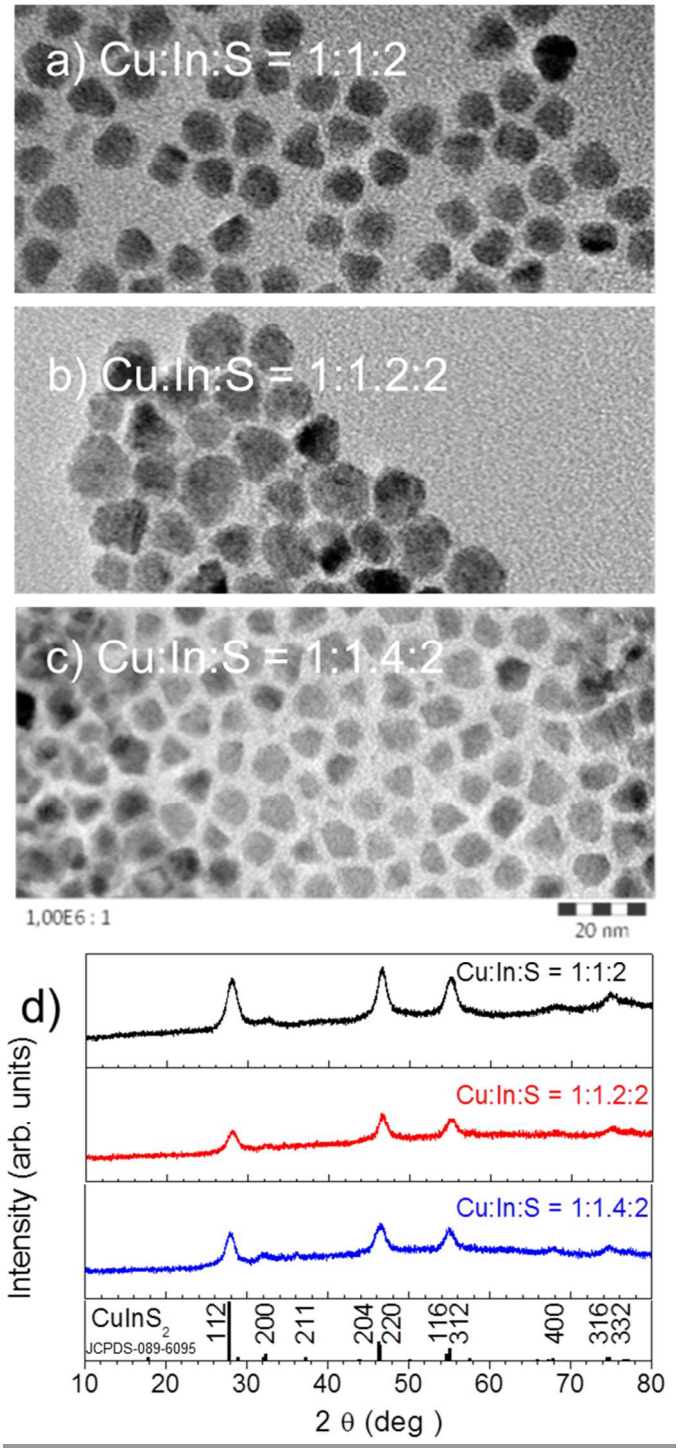

Figure 2. TEM images and X-ray diffractograms of CIS nanoparticles prepared with different precursor ratios of $[Cu(acac)_2]$:$[In(acac)_3]$:S, i.e. 10:10:20 mmol (a), 10:12:20 mmol (b) and 4.0:5.6:8.0 mmol (c) and XRD powder analyses of the respective samples (d). The PDF 089-6095 reference spectrum for $CuInS_2$ is added at the bottom.

The formation of tetragonal CIS (JCPDS No. 089-6095) was evidenced for each sample by XRD analysis (Figure 2 (d)) with no differences in the XRD signals between the samples. The main diffraction peaks along (112), (220)/(204), and (312)

direction, respectively, clearly indicate the structure of chalkopyrite $CuInS_2$. No other crystalline phases of CIS could be detected.

TEM images (Figure 2 (a,b,c)) show that independently from their composition CIS nanoparticles are formed in these syntheses with diameters ranging from 7 to 14 nm. The crystallinity and tetragonal crystal phase of the nanocrystals was further shown by high resolution TEM analysis (see ESI Figure S2). All CIS nanoparticles prepared are very well dispersable in toluene independently of their composition and do not show indication for a different behavior during the ligand exchange.

Scale up of $CuInS_2$ nanoparticle preparation

We further investigated the possibility to scale up the synthesis of $CuInS_2$ nanoparticles according to the present protocol. The amounts of the starting materials were increased five times (i.e., $[Cu(acac)_2]$:$[In(acac)_3]$:S = 50:50:100 mmol) at a reaction time of 120 minutes. The yield of CIS nanoparticles was approximately 11 g. TEM and X-ray analyses showed that the nanoparticles are comparable to those obtained from the synthesis at smaller scale, i.e. $CuInS_2$ nanoparticles of tetragonal crystalline structure with an average diameter of 14 nm (see ESI, Figure S3).

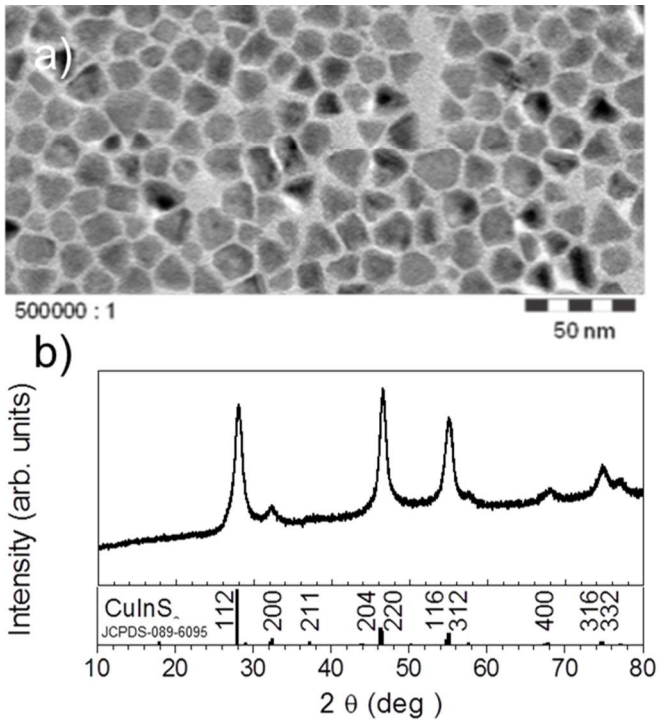

Figure 3. TEM image (a) and XRD powder analyses (b) of CIS nanoparticles, prepared at 11g scale (precursor ratio $[Cu(acac)_2]$:$[In(acac)_3]$:S = 50:50:100 mmol). The PDF 089-6095 reference spectrum for $CuInS_2$ is added at the bottom.

Ligand exchange

Prior to preparation of a photovoltaic sample surface ligand exchange of the as-synthesized nanoparticles was performed. The as-synthesized CIS nanoparticles contain the long-chain ligand oleylamine for the sake of their colloidal stability in dispersion. However, in a nanoparticle-based photovoltaic application, it is necessary to remove as much as possible of this long-chain ligands prior to film formation and sintering, which is achieved by a surface ligand exchange to a short carbon chain ligand, pyridine or allylamine in this study. Any long chain ligand obstacles charge transfer within the active layer of the photovoltaic and may hinder proper crystallization and film formation. The surface modification of CIS nanoparticles applied followed the recipe, which has been reported by Dilek et al..[18]

Selenized layers and solar cells

Various nanoparticles and ink formulations were tested for absorber formation and solar cell fabrication. However, we focus on the best process in the following using CIS nanoparticles that were synthesized at the Cu:In:S precursor ratio of 1:1:2 (Table 1, sample 1). The CIS nanoparticles were washed in methanol and hexane, followed by a pyridine ligand exchange and redispersed in pure pyridine at a solid content of 218 mg/ml (process (I)). TEM analysis of the material obtained showed that the nanoparticles were much closer to each other after this treatment (see ESI Figure S4), which may serve as valuable evidence for the successful replacement of the long chain oleylamine ligand by pyridine (a comprehensive discussion on this procedure for nanoparticle surface ligand exchange - as investigated on CdSe nanorods by thermogravimetry - is given in reference [[18]]). This ink was then deposited on Mo coated substrates by doctor blading, leading to a Cu:In ratio of 0.9 in the as-deposited precursor film as determined by XRF.[22] The ink showed good wettability and suitable viscosity to achieve homogenous layers during coating. Figure 4 (a) shows the as-deposited layer where grainy aggregates of CIS particles can be distinguished. In Figure 4 (b) a slight densification can be seen after the (incomplete) selenization step.

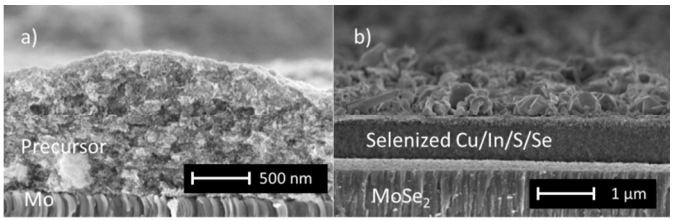

Figure 4. a) Cross section SEM image of an as-deposited layer made from a CIS-particle dispersion. b) similar layer after incomplete selenization: The absorber layer has undergone a densification.

However, drying of the films may become a critical factor regarding uncontrolled crack formation if the layers exceed a certain thickness. Figure 5 (a) shows a precursor layer of ~ 2 µm thickness, which after drying exhibited several cracks. The size of the cracks is correlated with the thickness of the wet layer. Correspondingly, the rather poor but still remarkable

power conversion efficiency (PCE) of 2.8% was obtained from this solar cell despite the optically poor appearance and the expectable high density of electrical shorts. Figure 5 (b) shows the cross section of the same layer after selenization, indicating that the detrimental cracks have been healed to some extend during selenization. To avoid crack formation, a thickness of 300-400nm turned out to be optimal as indicated by the crack-free layer shown in Figure 6 (a). Consequently, the efficiency obtained from the corresponding solar cell is clearly higher, reaching up to 6.1 %.

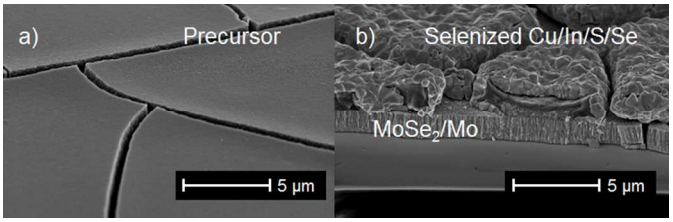

Figure 5. SEM images of a thick precursor layer (~ 2 µm in thickness) showing large crack formation (a) and of a similar layer after selenization (b).

In general, during the selenization step, which is conducted at high temperatures (550°C), a densification of the layers due to the lattice expansion upon sulfur replacement by selenium is observed and also large CISSe crystals start to grow on top of a small grained bottom layer. This effect is already visible in Figure 4 (b), but more pronounced in Figure 6. After prolonged selenization the bottom layer is comparatively carbon-rich incorporating the residues of ligands and solvents. Typically a thick $MoSe_2$ layer forms underneath the absorber layer due to the harsh selenization condition that is necessary to convert the $CuInS_2$ precursor. However, even thick (~ 1 µm) $MoSe_2$ does not seem to be very detrimental for the cell performance as long as Mo is still left and the adhesion is uncritical. The chemical composition of selenized layers was difficult to determine by XRF or EDX because of the high Se signal coming from the thick $MoSe_2$ layers and the overlapping signals for Mo and S. However, the initial Cu:In ratio of the as-deposited layer stayed at 0.9 after the selenization (XRF value). Depth profiles by SNMS revealed a rather homogeneous distribution of Cu, In and Se throughout the crystalline top layer and only reduced amounts in the bottom layer (see. Figure 7). However, the latter exhibited a high carbon content of up to 75 at. % (not shown) and some residual sulfur accumulated in the back contact region (with a S/Se ratio of up to 0.3), as shown in Figure 7. Hence, the sulfur atoms contained in the $CuInS_2$ precursor layer are successfully replaced by Se in the crystalline structure, while residual contents are mainly present in the carbon reach bottom layer.

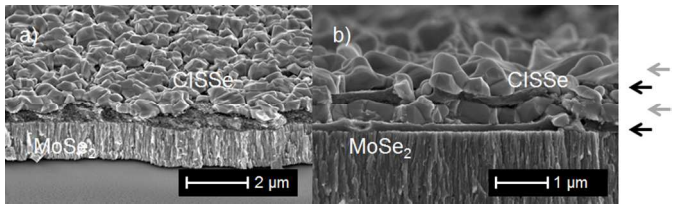

Figure 6. SEM images. a) Typical crack-free CISSe formation after selenization of a thin as-deposited $CuInS_2$ layer: large crystals on top of small-grained layer. b) Depending on the layer and selenization properties also alternating layers of different crystallinity can appear.

It should be mentioned that the formation mechanism during the selenization step is not fully understood, yet. Surprisingly in some cases not only a crystalline layer on a small-grain/carbon rich structure was observed, but also four layers of alternating crystal quality as demonstrated in Figure 6 (b, indicated by arrows). A lack of Se in the small-grained layer is unlikely as there are huge amounts of Se in the $MoSe_2$ layer underneath. Similarly, a blocking behaviour of the dense upper crystalline layer is disproved by the existence of an intermediate layer of high crystallinity in the structure of Figure 6 (b). The influence of the high carbon content in the bottom layer and the accompanying accumulation of residual sulfur may lead to this aggregation of separate layers.

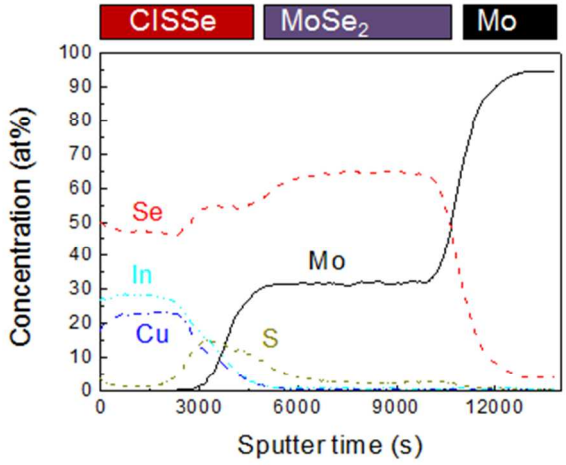

Figure 7. SNMS depth profile of element concentration of a CuInSSe absorber layer. A thick $MoSe_2$ layer is present on top of the Mo back contact layer. Carbon is not shown, but is highly accumulated at the back contact region between CISSe and $MoSe_2$.

The best power conversion efficiency was reached for a cell made from a CIS nanoparticle suspension with allylamine as surface capping ligand and chlorobenzene as solvent (process (II)). The selenized layers contributing to the complete solar cell stack are shown in Figure 8 (a), while the solar cell characterisitics are shown in Figure 8 (b). A PCE of 6.5 %, an open circuit voltage of 381 mV, a short circuit current density of 30.2 mA/cm^2 and a fill factor of 56 % were obtained for a typical Cu:In ratio of 0.9 (XRF).

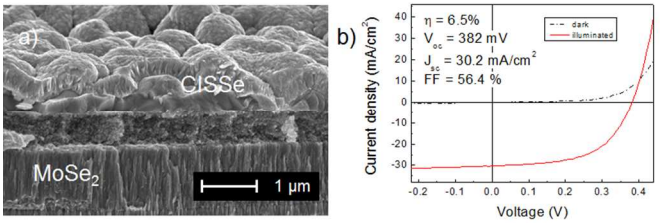

Figure 8. a) SEM image of best absorber layer after selenization under Se vapour at 550°C during 3 min showing the typical bilayer film formation characterized by a layer with large grains on top of a particle-like layer. b) Current-voltage characteristics of the corresponding solar cell with a PCE of 6.5%.

Conclusion

A simple route for the preparation of $CuInS_2$ nanoparticles in gram scale from $[Cu(acac)_2]$, $[In(acac)_3]$ elementary sulfur and oleylamine was developed. The $CuInS_2$ nanoparticles obtained have well defined sizes in the range of 7-14 nm and a thickness of approximately 5 nm. It was found that on injection of elementary sulfur into a $[In(acac)_3]$, $[Cu(acac)_2]$, oleylamine precursor mixture CuS nanoparticles form initially, which then slowly transform into the final tetragonal $CuInS_2$ phase. The In content of the nanoparticles can be varied by variation of the Cu:In precursor ratio. Pyridine or allylamine were successfully applied as surface exchange ligands prior to solar cell fabrication without notable reduction of the nanoparticle's dispersibility. Smooth crack-free layers were prepared from the $CuInS_2$ precursor inks and transformed into quaternary $CuIn(S,Se)_2$ absorber layers by selenization in pure selenium atmosphere giving solar cells with a PCE of up to 6.5%.

Acknowledgements

The authors are grateful to the German Ministerium für Bildung und Forschung (BMBF) for funding within the project "Nanopartikuläre Dünnschicht-Solarzellen − Grundlagen und Prozesstechnologie (NanoPV)" with the corresponding contract number 03SF0363. Support with sample preparation by D. Müller and A. Nowitzki is thankfully acknowledged. Furthermore, the authors thank F. Rauscher and C. Feldmann for fruitful discussions as well as R. Goerke for support in experimentation.

Notes and references

[a] Bayer Technology Services GmbH, D-51368 Leverkusen, Germany. Fax: +49-214-30-81118; Tel: +49-214-30-20053; E-mail: stefan.roggan@bayer.com.

[b] Zentrum für Sonnenenergie- und Wasserstoff-Forschung Baden-Württemberg (ZSW), D-70565 Stuttgart, Germany. Fax: +49-711-7870-230; Tel: +49-711-7870-0; E-mail: erik.ahlswede@zsw-bw.de

present address: Karlsruhe Institute of Technology (KIT), D-76131 Karlsruhe, Germany.

Electronic Supplementary Information (ESI) available: S1. TEM records of CIS samples obtained after 30 – 60 – 90 min reaction time (at Cu:In:S = 1:1:2 precursor ratio); S2. HRTEM of typical CuInS2 sample prepared with Cu:In:S = 1:1:1 precursor ratio; S3. Statistical size analysis of large scale CIS sample shown in Figure 3; S4. TEM images of as synthesized CIS sample and after surface ligand exchange with pyridine (at Cu:In:S = 1:1:2 precursor ratio). See DOI: 10.1039/b000000x/

1 a) http://www.zsw-bw.de/en/support/press-releases/press-detail/zsw-brings-world-record-back-to-stuttgart.html; b) P. Jackson, D. Hariskos, R. Wuerz, W. Wischmann and M. Powalla, *Phys. Status Solidi RRL* **2014**, *8*, 219

2 A. M. Gabor, J. R. Tuttle, D. S. Albin, M. A. Contreras, R. Noufi and A. M. Hermann, *Appl. Phys. Lett.* **1994**, *65*, 198.

3 M. Marudachalam, H. Hichri, R. Klenk, R. W. Birkmire, W. N. Shafarman and J. M. Schultz, *Appl. Phys. Lett.* **1995**, *67*, 3978.

4 V. Probst, W. Stetter, W. Riedl, H. Vogt, M. Wendl, H. Calwer, S. Zweigart, K.-D. Ufert, B. Freienstein, H. Cerva and F. H. Karg, *Thin Solid Films* **2001**, *387*, 262.

5 M. Kaelin, D. Rudmann and A. N. Tiwari, *Sol. Energy* **2004**, *77*, 749.

6 C. J. Hibberd, E. Chassaing, W. Liu, D. B. Mitzi, D. Lincot and A. N. Tiwari, *Prog. Photovolt., Res. Appl.* **2010**, *18,* 434.

7 T. Todorov and D. B. Mitzi, *Eur. J. Inorg. Chem.* **2010**, 17.

8 T. Todorov, O. Gunawan, T. Gokmen and D. Mitzi, *Prog. Photovoltaics* **2013**, *21*, 82.

9 G. Brown, P. Stone, J. Woodruff, B. Cardozo and D. Jackrel, *38th IEEE Photovoltaic Specialists Conference* **2012**, 3230.

10 J. Hedstrom, H. Ohlsen, M. Bodegard, A. Kylner, L. Stolt, D. Hariskos, M. Ruckh and H. Schock. *23rd IEEE Photovoltaic Specialists Conference* **1993**, 364.

11 J. A. M. AbuSharma, S. Johnston, T. Moriarty, G. Teeter, K. Ramanathan and R. Noufi *Prog. Photovoltaics* **2004**, *12,* 39.

12 W. Liu, D. B. Mitzi, S. J. Chey and A. Kellock, *Mater. Res. Soc. Symp. Proc.* **2009**, *1123*, P06-03-F07-03.

13 G. Norsworthy, C. R. Leidholm, A. Halani, V. K. Kapur, R. Roe, B. M. Basol and R. Matison *Sol. Energ. Mat. Sol. Cells* **2000**, *60,* 127.

14 Q. Guo, G. M. Ford, H. W. Hillhouse, R. Agrawal, *Nano Lett.* **2009**, *9*, 3060.

15 C. J. Stolle, T. B. Harvey and B. A. Korgel, *Current opinion in chemical engineering* **2013**, *2*, 1.

16 H. Azimi, Y. Hou and C. J. Brabec, *Energy Environ. Sci.* **2014**, *7*, 1829.

17 M. G. Panthani, V. Akhavan, B. Goodfellow, J. P. Schmidtke, L. Dunn, A. Dodabalapur, P. F. Barbara and B. A. Korgel *J. Am. Chem. Soc.* **2008**, *130*, 16770.

18 D. Celik, M. Krueger, C. Veith, H. F. Schleiermacher, B. Zimmermann, S. Allard, I. Dumsch, U. Scherf, F. Rauscher and P. Niyamakom *Solar Energy Mater. Solar Cells* **2012**, 98, 433.

19 M. Powalla and B. Dimmler, *Thin Solid Films* **2001**, *387*, 251.

20 C. Shen, C. Hui, T. Yang, C. Xiao, J. Tian, L. Bao, S. Chen, H. Ding and H. Gao, *Chem. Mater.* **2008**, *20*, 6939.

21 a) M. Kruszynska, H. Borchert, J. Parisi and J. Kolny-Olesiak, *J. Am. Chem. Soc.* **2010**, *132*, 15976; b) J. Kolny-Olesiak, *CrystEngComm*. **2014**, *16*, 9381; c) J. Li, M. Bloemen, J. Parisi, and J. Kolny-Olesiak, *ACS Appl. Mater. Interfaces* **2014**, *6*, 20535.

22 There is a slight discrepancy in the composition values determined by ICP or XRF.

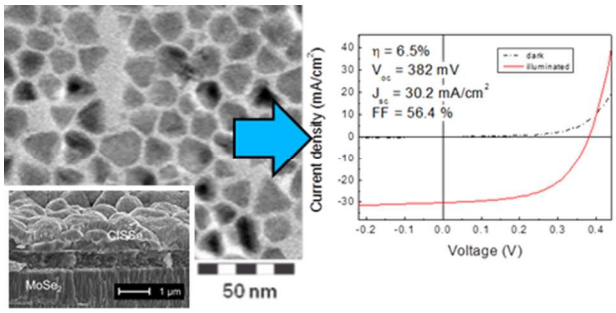

Investigation of an scalable synthesis of chalcopyrite $CuInS_2$ nanoparticles comprising composition, growth mechanism, surface ligand exchange and solar cell fabrication.